Proceedings of the ASME 2010 3rd Joint US-European Fluids Engineering Summer Meeting and 8th International Conference on Nanochannels, Microchannels, and Minichannels
FEDSM-ICNMM2010
August 1-5, 2010, Montreal, Canada

FEDSM-ICNMM2010-30491

ACTIVE FLOW CONTROL OF THE 3D SEPARATION ON A AHMED BODY USING STEADY MICROJET ARRAYS

S. Aubrun
Institut PRISME,
Université d'Orléans,
8 rue Léonard de Vinci, F-45072 Orléans, France

F. Alvi
FAMU-FSU College of Engineering,
Florida State University,
2525 Pottsdamer Str., Tallahassee, FL32310, USA

A. Leroy
Institut PRISME,
Université d'Orléans,
8 rue Léonard de Vinci, F-45072 Orléans, France

A. Kourta
Institut PRISME,
Université d'Orléans,
8 rue Léonard de Vinci, F-45072 Orléans, France

ABSTRACT
A model of a generic vehicle shape, the Ahmed body with a slant angle of 25°, is equipped with an array of blowing steady microjets 6mm downstream of the separation line between the roof and the slanted rear window. The goal of the present study is to evaluate the effectiveness of this actuation method in reducing the aerodynamic drag, by reducing or suppressing the 3D closed separation bubble located on the slanted surface. The efficiency of this control approach is quantified with the help of aerodynamic load measurements. The changes in the flow field when control is applied are examined using PIV measurements and skin friction visualizations. By activating the steady microjet array, the drag coefficient was reduced by 9 to 11%, depending on the Reynolds number. The modification of the flow topology under progressive flow control is particularly studied.

NOMENCLATURE
C_D Drag coefficient
C_L Lift coefficient
C_μ Steady momentum coefficient
$C_{\mu,c}$ Critical steady momentum coefficient
Q_v Total volume flow rate of the microjet array
$Q_{v,c}$ Critical volume flow rate of the microjet array
Re_L Reynolds number based on Ahmed body length
V_{jet} Microjet exit velocity
U_∞ Freestream reference velocity
W Ahmed body width
δ Boundary layer thickness at the sharp edge

INTRODUCTION
Several active flow control techniques have been found to reduce or even to suppress a 3D separation. One can cite the steady blowing or suction of air flow through slits or holes [1, 2], the array of unsteady (synthetic or pulsed) jets [3], the steady or unsteady plasma actuators [4, 5]. All of these methods offer some advantages and drawbacks. The steady blowing or suction through orifices distributed along a line normal to the freestream flow and located close downstream of the separation line has been shown to be efficient in re-attaching the flow and is also one of the simplest actuator, from a practical and implementation point of view. These devices require a continuous supply or intake of mass flow through such orifices. In the case of slits, the mass flow rate has been shown to be very high in order to obtain a control effect. On the other hand, the use of array of steady microjets instead of one slit is seen as more economic regarding the supplying flow rate. Furthermore, the physical mechanisms behind this 'discrete' or 'segmented' control differ from the use of slits. Steady microjets act as 3D disturbances which generate distinct 3D structures which offer some advantages in terms of mixing or reenergizing the separating boundary layer [6, 7]. In the context of automotive applications, the perspective of reducing the vehicle drag with the use of flow control is considered. The steady blowing actuators being considered here are serious contenders since they are based on a simple and proven technology. The main potential drawback of this actuator is the need of a mass flow supply; in principal this may by addressed by designing a system which may capture some mass flow through strategically-located intakes in the vehicle and release the flow

through the actuators. In addition, by optimizing the placement and design of these actuators, the mass flow rate may also be significantly reduced.

To study the efficiency of this approach for automotive configurations, a model of a generic shape of a vehicle, the Ahmed body with a slant angle of 25° [8], is equipped with a row of steady microjets 6mm downstream of the separation line between the roof and the slanted rear window (see side—view schematic in Fig. 1). Here, a 3D closed separation bubble is generated on the slanted surface due to the sharp edge between the roof and the slanted surface [8]. The efficiency of the device is quantified with the help of aerodynamic load measurements. The modification to the flow field when control is applied is studied by using PIV measurements and skin friction visualizations. The goal of the present study is to evaluate the topology modification under progressive flow control efficiency.

EXPERIMENTAL SET-UP

The Ahmed body model (Fig. 1) at a geometric scale of 0.7 (the full scale is related to the historical body studied by Ahmed [8]) is studied in the “Lucien Malavard” wind tunnel of the PRISME Institute, University of Orléans (Fig. 2). The test section is 2m high, 2m wide and 5m long. The maximum freestream velocity in the tunnel is 60m/s, the freestream turbulence intensity is below 0.3% and the mean flow homogeneity is 0.5% along a transverse distance of 1200mm. The model is installed on a 6-axis aerodynamic balance using its 4 feet that are 20mm in diameter and are fixed to a horizontal metallic frame. This frame is mounted on a 2m wide and 3m long flat plate located at 480mm above the wall of the wind tunnel, which enables the development of a new, thin, boundary layer upstream and below the model. The flat leading edge is elliptic and its trailing edge is controllable in order to suppress the longitudinal pressure gradient in the test section. The thickness of the boundary layer, which is developing on the plate, has been measured at the model location for a freestream velocity of 30m/s, it is 20mm whereas the distance between the plate and the bottom of the model is 50mm.

For an upstream velocity of U_∞ = 40m/s, the boundary layer at the edge between the roof and the slanted edge is turbulent and δ = 13mm thick.

The actuator is composed of 53 holes, 0.4mm in diameter and regularly spaced along a line parallel to the sharp edge between the roof and the rear window. This actuator array is 6mm downstream of the sharp edge and the space between the microjets is 5mm. The microjet holes are drilled in a parallelepiped chamber of 272mm wide, 4.8mmhigh and 9.5mm long, which is embedded in the rear window. Air is supplied to the chamber through 4 supply ports that are all connected to a single manifold. The manifold is connected to a pressure supply with a maximum capacity of 3bars. The flow rate through the actuators is controlled through a vertical rotameter and the total pressure in the chamber is measured against a reference pressure (atmospheric pressure, or freestream static pressure in the wind tunnel, or static pressure somewhere on the rear window) with a differential pressure transducer DRUCK LPM (range 0 to 1bar). The flow rate used during the measurement campaign is from Q_v = 0 to 3.7m^3/h. The maximum exit velocity at each single hole is then assessed to up to V_{jet} = 155m/s.

For an upstream velocity of U_∞ = 40m/s, one can deduce that the associated steady momentum coefficient C_μ is between 1.1% and 5.7% with :

$$c_\mu = \frac{\rho_{air}\, Q_v\, U_{jet}}{0.5\,\rho_{air}\, U_\infty^2\, W\,\delta} \quad (1)$$

This steady momentum coefficient indicates the ratio of magnitude of total momentum injected by the actuator into the flow relative to the freestream dynamic pressure multiplied with an appropriate area $W\delta$, where W is the Ahmed body width and δ, the boundary layer thickness at the sharp edge between the roof and the rear window. It represents the fraction of the momentum flux which is added to the flow compared to the baseline momentum flux through a relevant surface based on the specific configuration (here, the boundary layer along the span of the body) [6-7].

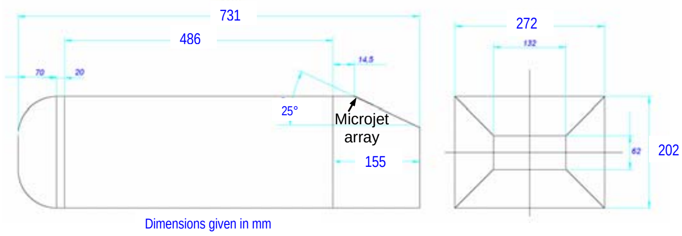

FIGURE 1: AHMED BODY AT A GEOMETRIC SCALE OF 0.7, WITH A SLANT ANGLE BETWEEN THE ROOF AND THE REAR WINDOW OF 25°.

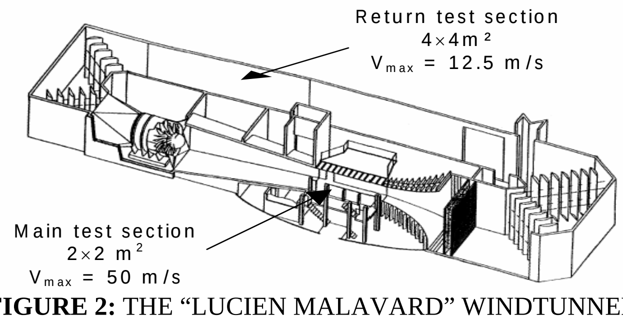

FIGURE 2: THE “LUCIEN MALAVARD” WINDTUNNEL OF THE INSTITUT PRISME, UNIVERSITY OF ORLEANS

Aerodynamic loads are measured with a 6-axis balance located below the test section. A mast of 30mm of diameter is used to link the balance to the metallic frame on which, the model is fixed. The precision of the balance is assessed to be

0.1N for the drag measurement and 0.3N for the lift. Some tests were performed to quantify the drag and lift forces induced by the actuating steady jets without any freestream flow. For flow rates up to 3m^3/h, the measured loads were within the balance precision. They can be then considered as negligible.

Friction line visualisations on the slanted edge and on its side are performed using a viscous coating made of oleic acid, dodecane, silicon oil and titanium dioxide [9]. The wall is coated with the mixture using a brush, the model is then exposed to a constant wind until the friction lines become visible.

Two-component PIV measurements are performed in the vertical plane of symmetry of the body, on the rear window and in the near wake of the body. A Nd :Yag laser (QUANTEL ultra 200) generating 2 pulses of 200mJ each at a wavelength of 532nm is located above the test section. A streamwise slit in the roof enables the vertical laser light sheet to reach the model. The optical set-up is chosen to generate a sheet as thin as possible in the proximity of the model. Images are captured with a CCD TSI Power View Plus camera (2048 x 2048 pixels) located outside the test section, on one side of the wind tunnel. The complete tunnel circuit is seeded with micro-sized droplets of olive oil generated by a PIVTEC seeding system. The laser and the camera are synchronised by a TSI synchroniser and the image processing is performed with Insight3G. Dimensions of the PIV images are 210mm x 210mm. Interrogation windows of 16 x 16 pixels are used with an overlap of 50%. 500 pairs of images are captured for each configuration tested.

AERODYNAMIC LOADS

Figure 3 shows the drag coefficient, C_D, of the Ahmed body as a function of the steady momentum coefficient supplied through the steady microjet array. Results are shown for three Reynolds numbers, based on the freestream velocity and the length of the model. The efficacy of flow control is visible for all cases, where a decrease of 8 to 11% in the drag coefficient appears for each configuration. The critical steady momentum coefficient $C_{\mu,c}$ above which the actuator becomes effective (chosen for a drag reduction equal to the half of the total drag reduction), is thus similar for each Reynolds number and is between 1.2% and 1.5%. Above this critical value, the efficiency of the control is nearly constant since the drag coefficient stays constant.

Figure 4 presents the lift coefficient C_L for the same three cases. It is interesting to see that the optimal control (defined here as the configuration where the maximum decrease of drag coefficient is obtained, is also associated with a strong decrease in lift (up to 42%). On the other hand, it is interesting to note that as the C_μ increases, although control remains effective in decreasing drag, the lift force begins to increases again. It indicates that, even though drag control appears constant, the flow topology around the rear-part of the Ahmed body is still under evolution. This aspect is examined using velocity field measurements and friction line visualizations, discussed next.

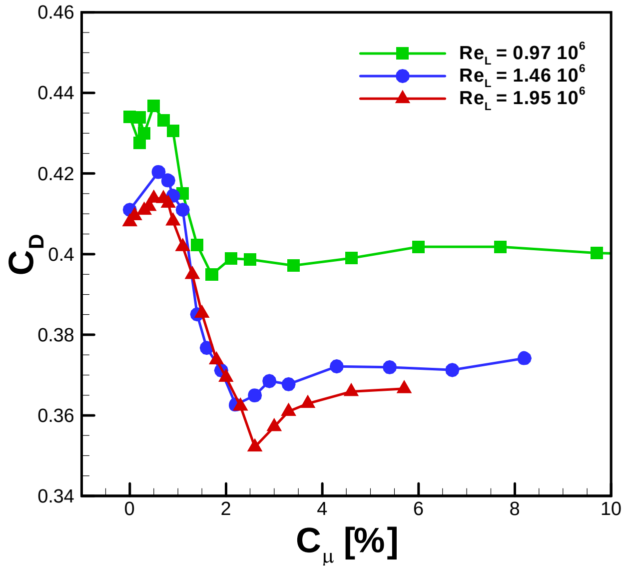

FIGURE 3: DRAG COEFFICTIENT VERSUS STEADY MOMENTUM COEFFICIENT FOR DIFFERENT Re_L.

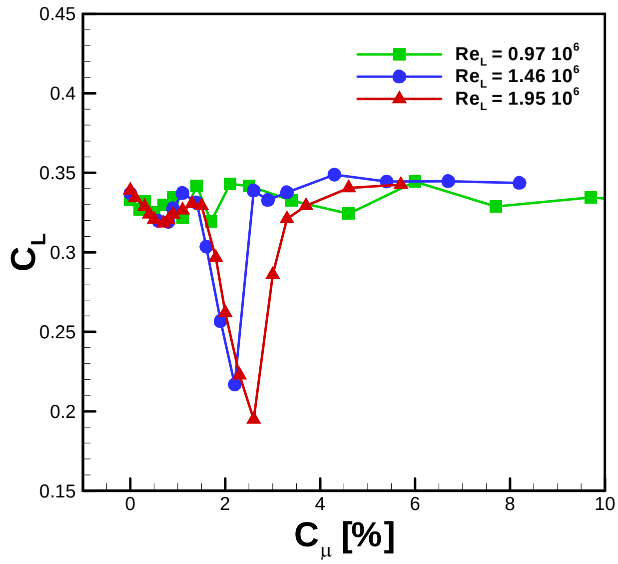

FIGURE 4: LIFT COEFFICTIENT VERSUS STEADY MOMENTUM COEFFICIENT FOR DIFFERENT Re_L.

FLOW TOPOLOGY ON THE REAR OF THE AHMED BODY

PIV measurements on the vertical middle plane and friction line visualizations over the slanted surface are performed in order to study the flow field modifications under progressive flow control. Only the case corresponding to $\boldsymbol{Re_L}$=1.95 10^6 is analysed.

Figure 5 shows the mean velocity magnitude fields non-dimensioned by the freestream velocity $\boldsymbol{U_\infty}$ and the associated friction line visualizations for different steady momentum coefficients. Except for the maximum control configuration, the recirculation is visible on both representations. Friction line visualizations show that the separation is strongly 3D and that the signature of the steady streamwise vortical structure at both sides of the rear window, characterised by a nearly straight detachment line, is obvious. According to these visualizations, the structures are not modified by this particular control. This result is in agreement with Thacker et al [10] since they showed that, suppressing the closed separation bubble on the 25° slanted edge of an Ahmed body by rounding the edge between the roof and the rear window did not modify the properties of the trailing vortices. On the other hand, Aider et al. [11] showed different results when they control the separation on a significantly modified Ahmed body with a curved rear part, they suggest that the drag reduction could be due to the breakdown of the balance between the separation bubble and the trailing longitudinal vortices. It is obviously not the case in our configuration.

In areas where the flow under control is attached, the microjet signatures are visible all along the slanted surface. It proves that the flow structures generated thanks the microjet efficacy stay very close to the wall and keep coherence and strength along a far distance.

Without control, the separated shear layer reattaches on the slanted surface and the maximum separation length, located at the symmetry plane, is 2/3 of the slanted surface length.

As the control is progressively acting (from $\boldsymbol{C_\mu}$ = 1.5%), the flow is fully reattached on lateral parts of the slanted surface but a very complex 3D separation still subsists at the centre of the surface. From $\boldsymbol{C_\mu}$ = 2%, the separation point is not fixed at the sharp edge anymore, but is progressively shifted downstream of the actuator location. At the same time, the reattachment zone is not entirely located on the slanted surface anymore, leading to a separation opened to the rear base wake flow.

It is the reason why the lift coefficient is particularly affected by the control for these intermediate $\boldsymbol{C_\mu}$ values, since the associated flow topology indicates a link between the rear base and the rear window flows, leading to a static pressure equilibrium between both zones. The associated decrease of lift and drag forces indicates that the static pressure on the rear window should be risen up.

For steady momentum coefficients $\boldsymbol{C_\mu}$ > 3%, the separation is totally suppressed on the slanted surface, the drag coefficient is stabilised and the lift coefficient is again similar to the configuration without control. It proves that the natural separation on the rear window contributes a few to the lift force.

The flow and pressure field properties need to be further examined, a process that is continuing, to shed more light into the coupling of the flow properties with aerodynamic loads and their response to the present control approach.

CONCLUSIONS

The present study shows that the use of an array of steady microjets, downstream and in the vicinity of the sharp edge between the roof and the rear window of an Ahmed body is very effective in controlling the separation bubble located on the rear window. Indeed, the drag coefficient was reduced to 9 to 11%, depending on the Reynolds number. It was also shown that once the optimal steady momentum coefficient $\boldsymbol{C_\mu}$ (defined as the configuration where the maximum decrease of drag coefficient is obtained with the minimum $\boldsymbol{C_\mu}$) is reached, the drag reduction remains constant. On the other hand, the lift coefficient shows a different evolution. It continues to drop up to a maximum of 42% (reduction) corresponding to the optimal flow rate case; however, it begins to increase again until it reaches its original value (without control) as the actuator flow rates are further increased. These results indicate that it is possible to reach the same efficiency, with respect to drag alone, with different flow topologies.

Flow fields measurements in the vertical plane of symmetry of the model were combined with friction line visualizations on the rear window in order to better elucidate the differences in flow topology on the rear window under progressive control.

Observations of flow topology confirm that the separation area on the rear window is a very complex 3D structure. As the control efficacy is increasing, the separation point is progressively shifted to farther downstream positions, leading to a drag force decrease, and the separation does not reattach on the rear base anymore. It is then linked to the rear base wake flow, leading to a lift force decrease.

It was also noticeable that, in areas where the flow under control is attached, the microjet signatures are visible all along the slanted surface. It proves that the flow structures generated thanks the microjet efficacy stay very close to the wall and keep coherence and strength along a far distance.

This study is an initial part of an ongoing project where several additional experiments are planned. Future studies include unsteady pressure measurements on the rear window and on the rear base in order to characterise the influence of this steady flow control on the unsteady flow properties. A detailed characterisation of the single working microjet will be performed using high-resolution PIV (entire image field of a few centimetres) in a transverse plane aligned to the jet direction. These and other additional measurements will shed more light on the mechanisms responsible of the suppression of the separation bubble and the global flow topology thus helping us further improve this control approach from a practical perspective.

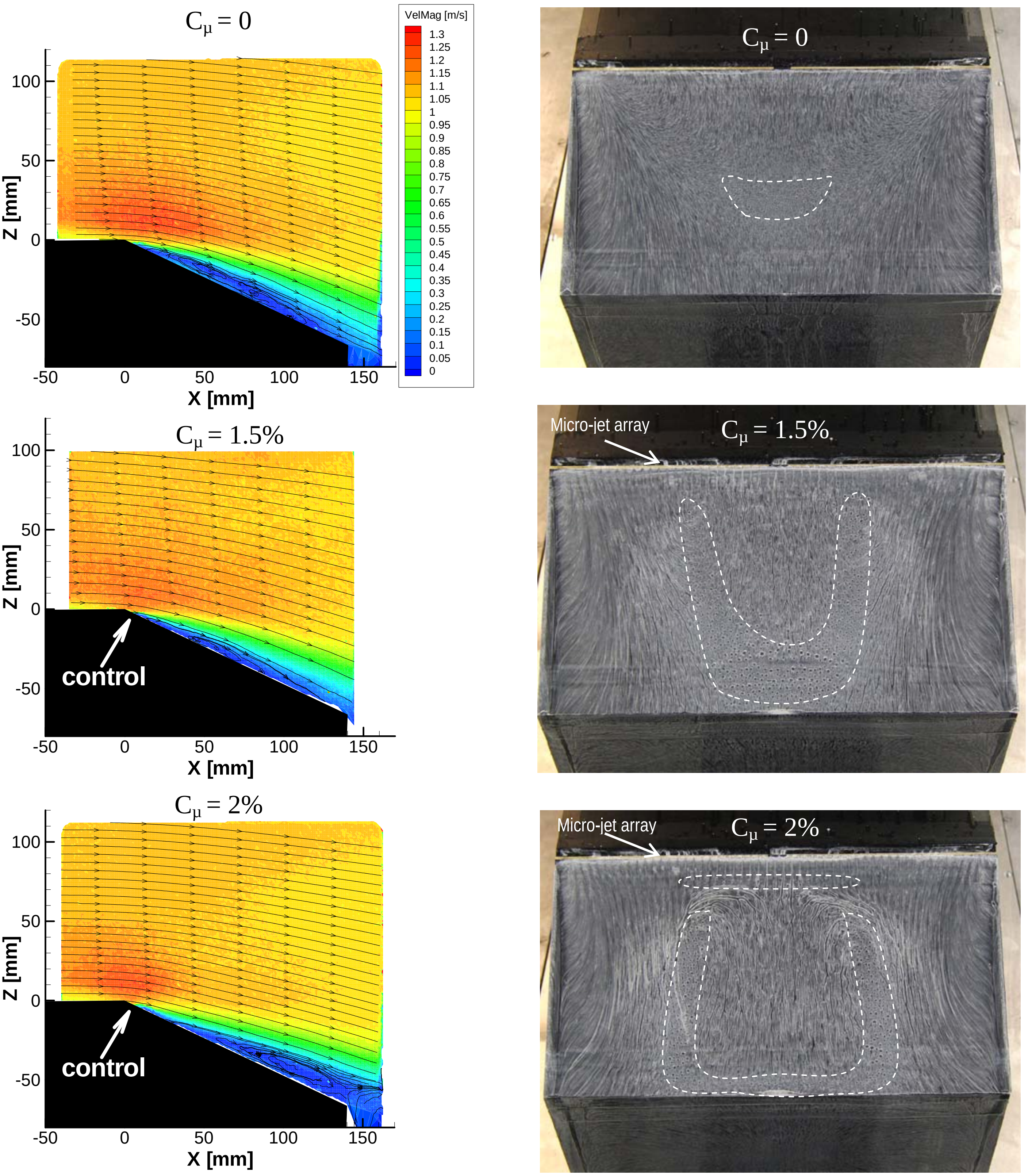
Cμ = 0
VelMag [m/s]
1.3
1.25
1.2
1.15
1.1
1.05
1
0.95
0.9
0.85
0.8
0.75
0.7
0.65
0.6
0.55
0.5
0.45
0.4
0.35
0.3
0.25
0.2
0.15
0.1
0.05
0
Z [mm]
X [mm]
Cμ = 1.5%
control
Cμ = 2%
Micro-jet array

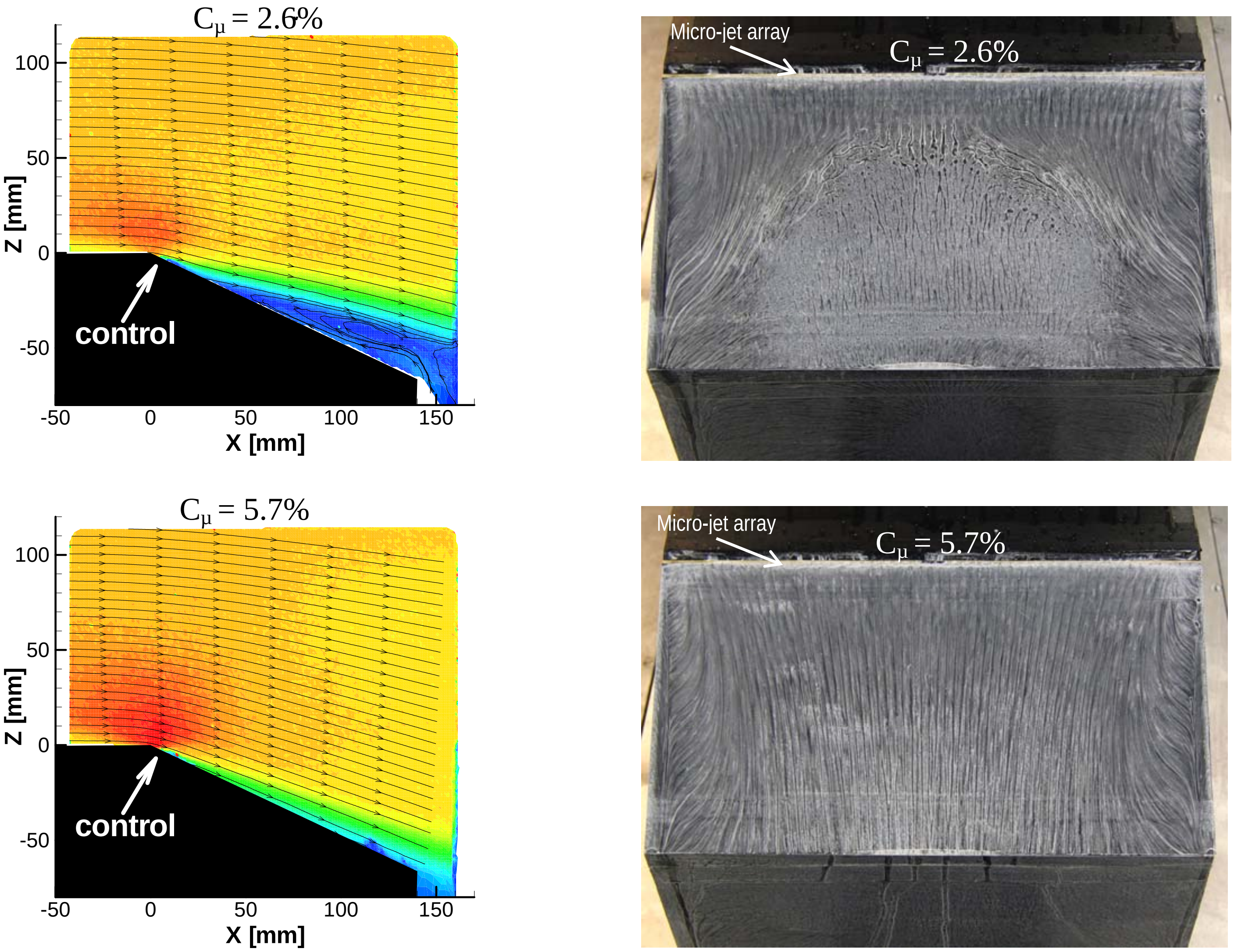

FIGURE 5: DIMENSIONLESS MEAN VELOCITY MAGNITUDE WITHIN THE VERTICAL PLANE OF SYMMETRY OF THE BODY. ON THE REAR WINDOW.(LEFT) AND SKIN FRICTION VISUALIZATIONS ON THE REAR WINDOW (RIGHT). DASHED LINES SHOW STAGNATION AREAS. RE_L.= 1.95 10^6

REFERENCES

[1] J. Favier, L. Cordier, A. Kourta, « Sur l’optimisation d’actionneurs pour le contrôle d’écoulements », Mécanique & Industries 8, n° 3, 259-265, 2007.

[2] M. Rouméas, P. Gilliéron, A. Kourta, “Drag reduction by flow separation control on a car after body”, Int. J. Numer. Meth. Fluids 2009; **60**:1222–1240

[3] Leclerc C.; « Réduction de la traînée d'un véhicule automobile simplifié à l'aide du contrôle actif par jet synthétique », thèse doctorat, CIFRE Renault/Institut de Mécanique des Fluides de Toulouse, janvier 2008.

[4] V. Boucinha, P. Magnier, A. Leroy-Chesneau, R. Weber, B. Dong et D. Hong, “Characterization of the Ionic Wind Induced by a Sine DBD Actuator used for Laminar-to-Turbulent Transition Delay by LDV”, 4th AIAA Flow Control Conference, Seattle (USA), 23-26/06-2008

[5] V. Boucinha, R. Joussot, P. Magnier, R. Weber et A. Leroy-Chesneau, “Characterization of the ionic wind produced by a DBD actuator designed to control the laminar-to-turbulent transition”, 14th International Symposium on applications of Laser Techniques to Fluid Mechanics, Lisbonne (Portugal), 07-10/07 2008 (acts on CD)

[6] Kumar V. and Alvi F, “Use of High-Speed Microjets for Active Separation Control in Diffusers”. AIAA Journal Vol. 44, n°2, pp. 273-281, 2006.

[7] Kumar V. and Alvi F., “Towards Understanding and Optimizing Separation Control Using Microjets. AIAA Journal 2009 0001-1452 vol.47 no.11 (2544-2557)

[8] Ahmed S. R., Ramm R. & Falting G., “Some salient features of the time averaged ground vehicle wake”, SAE technical paper series 840300, Detroit 1984

[9] Anne-Archard D., Du Colombier D., Boisson H., Herbert V., « Analyse des enduits de visualisation pariétale utilisés en aérodynamique », 41ème colloque National du Groupe Français de Rhéologie, 18-20 octobre 2006, Cherbourg, France

[10] Thacker A., Leroy A., Aubrun S., Loyer S., Devinant P.. « Caractéristiques du sillage du corps de Ahmed : Effet de la suppression du décollement de lunette arrière. »
Colloque du GDR2502 « Contrôle Des Décollements »,24-25 novembre 2009, Orléans. Cépaduès Editions, ISBN 978.2.85428.916.9. (2009), pp 87-94.

[11] Aider J.L., Beaudoin J.F., Wesfreid J.E. “Drag and lift reduction of a 3D bluff-body using active vortex Generators. Exp Fluids (2010) 48:771–789